

Drought Characteristics and Propagation in the Semiarid Heihe River Basin in Northwestern China

FENG MA

State Key Laboratory of Earth Surface and Ecological Resources, Faculty of Geographical Science, Beijing Normal University, Beijing, China, and Department of Geography, Environment, and Spatial Sciences, Michigan State University, East Lansing, Michigan

LIFENG LUO

Department of Geography, Environment, and Spatial Sciences, Michigan State University, East Lansing, Michigan

AIZHONG YE AND QINGYUN DUAN

State Key Laboratory of Earth Surface and Ecological Resources, Faculty of Geographical Science, Beijing Normal University, Beijing, China

(Manuscript received 21 June 2018, in final form 27 November 2018)

ABSTRACT

Meteorological and hydrological droughts can bring different socioeconomic impacts. In this study, we investigated meteorological and hydrological drought characteristics and propagation using the standardized precipitation index (SPI) and standardized streamflow index (SSI), over the upstream and midstream of the Heihe River basin (UHRB and MHRB, respectively). The correlation analysis and cross-wavelet transform were adopted to explore the relationship between meteorological and hydrological droughts in the basin. Three modeling experiments were performed to quantitatively understand how climate change and human activities influence hydrological drought and propagation. Results showed that meteorological drought characteristics presented little difference between UHRB and MHRB, while hydrological drought events are more frequent in the MHRB. In the UHRB, there were positive relationships between meteorological and hydrological droughts, whereas drought events became less frequent but longer when meteorological drought propagated into hydrological drought. Human activities have obviously changed the positive correlation to negative in the MHRB, especially during warm and irrigation seasons. The propagation time varied with seasonal climate characteristics and human activities, showing shorter values due to higher evapotranspiration, reservoir filling, and irrigation. Quantitative evaluation showed that climate change was inclined to increase streamflow and propagation time, contributing from -57% to 63% . However, more hydrological droughts and shorter propagation time were detected in the MHRB because human activities play a dominant role in water consumption with contribution rate greater than $(-)$ 89% . This study provides a basis for understanding the mechanism of hydrological drought and for the development of improved hydrological drought warning and forecasting system in the HRB.

1. Introduction

Drought is a complex phenomenon, and it originates from a deficiency of rainfall over a prolonged period of time, leading to water shortage in soil and hydrological system via hydrological cycle (Mishra and Singh 2010; Van Loon 2013, 2015; Wilhite 2000). Unlike other natural disasters, drought develops slowly and can have long-lasting impacts, which results in

severe economic, environmental, and societal problems worldwide (Seneviratne et al. 2012). Droughts are classified into four types, including meteorological (precipitation), agricultural (soil moisture), hydrological (streamflow and groundwater), and socioeconomic droughts (Mishra and Singh 2010; Wilhite 2000). Meteorological droughts are the origin of other types of droughts and can propagate to agricultural and hydrological droughts, which may result in socioeconomic losses (socioeconomic droughts; Eltahir and Yeh 1999; Van Loon 2013; Van Loon et al. 2014).

Corresponding author: Aizhong Ye, azye@bnu.edu.cn

DOI: 10.1175/JHM-D-18-0129.1

© 2019 American Meteorological Society. For information regarding reuse of this content and general copyright information, consult the [AMS Copyright Policy](https://www.ametsoc.org/PUBSReuseLicenses) (www.ametsoc.org/PUBSReuseLicenses).

The drought propagation from meteorology to hydrology has significant impacts on water resources management, which depends strongly on both climate and catchment characteristics (Van Loon and Van Lanen 2012). Therefore, hydrological drought features may display huge distinctions in different regions of the world, in spite of similar meteorological drought characteristics (e.g., number of events, duration, and severity; Van Loon et al. 2014). To better manage water resources and reduce the effects of droughts, understanding drought propagation and its influence factors is needed in a given region. A number of studies have investigated drought propagation at the regional scale (e.g., Barker et al. 2016; Hannaford et al. 2011; Huang et al. 2017) and focused on the effects of climate and catchment characteristics on drought propagation. However, the role of human activities on the propagation of drought has not been well explored, since human activities largely influence hydrological processes underlying drought characteristics and propagation, especially in human-dominated regions (Van Loon et al. 2016). The Heihe River basin, an endorheic river basin in northwest China, is an important region for agricultural production that is highly dependent upon irrigation with a history of approximately 2000 years (Lu et al. 2015). Overexploitation of water resources of this basin has changed the hydrological processes and consequently impacts the hydrological drought characteristics and drought propagation, especially in the midstream region.

This study assesses meteorological and hydrological drought characteristics and the propagation behaviors in the Heihe River basin using the standardized indicators (Farahmand and AghaKouchak 2015), that is, the standardized precipitation index (SPI) and standardized streamflow index (SSI). The study will address the following key questions:

- 1) How do meteorological and hydrological drought characteristics vary across the upstream and midstream of the Heihe River basin?
- 2) How do meteorological droughts propagate into hydrological droughts, and how is the process different between upstream and midstream of the Heihe River basin?
- 3) How and to what extent do climate change and human activities affect hydrological drought characteristics and propagation?

We aim to fill the gaps in quantitative analysis of effects of climate change and human activities on hydrological drought and drought propagation by addressing these questions. In section 2, the study area and data used in this study are described. Section 3 presents the methods for characterizing droughts and propagation behaviors and for separating effects of climate change

and human activities. Section 4 presents the results and discussion. Finally, conclusions are given in section 5. This work will provide an important foundation for the development of hydrological drought warning and forecasting systems based on climate predictions in the Heihe River basin, allowing for better drought preparedness in advance.

2. Study area and data

a. The upper and middle reaches of Heihe River basin

The Heihe River basin (HRB; 96°42′–102°E, 37°41′–42°42′N) is the second-largest inland river basin in the arid zone of northwestern China (Fig. 1). The total drainage area is 128 900 km², and its mainstream spans 821 km (Ma and Frank 2006). The elevation ranges between 800 and 5600 m, with significant topography varying from south to north (Wang et al. 2012). The HRB is divided into upstream (UHRB), midstream (MHRB), and downstream (DHRB) based on its climate and ecological characteristics (Liu et al. 2010; Qin et al. 2010). Among them, the upstream is from the Qilian Mountains to Yingluoxia Gorge, which is characterized by the mountainous terrains with alpine meadow. The midstream, from Yingluoxia Gorge to Zhengyixia Gorge, is characterized by oases with irrigated agriculture, and the downstream is mainly covered by the Gobi Desert with lower precipitation and higher evaporation (Li et al. 2001). The average annual rainfall in the UHRB, MHRB, and DHRB is 350–450 mm, 80–120 mm, and 40–60 mm, respectively, and average annual temperatures are from –3.1° to 3.6°C, 7°–8.2°C, and 8°–10°C, respectively (Pan et al. 2014). It should be emphasized that the midstream is a very important agricultural production zone, where agriculture plays a vital role in local economic growth. In this study, we focus on the UHRB and MHRB, considering agriculture and ecosystem in the midstream place heavy demands on water resources delivered from the upstream region. Most of the water resources in the HRB are generated from rainfall and glacier-snow melting in the UHRB (Wang et al. 2010).

b. Data

Daily precipitation data covering 1961–2015 at a 0.5° resolution were obtained from the National Meteorological Information Center, China Meteorological Administration (CMA; Zhao and Zhu 2015) and were interpolated from 2472 meteorological stations all over China using the thin plate spline method (Hutchinson 1998a,b). Daily temperature data were collected from 11 meteorological stations spanning 1961–2013, also

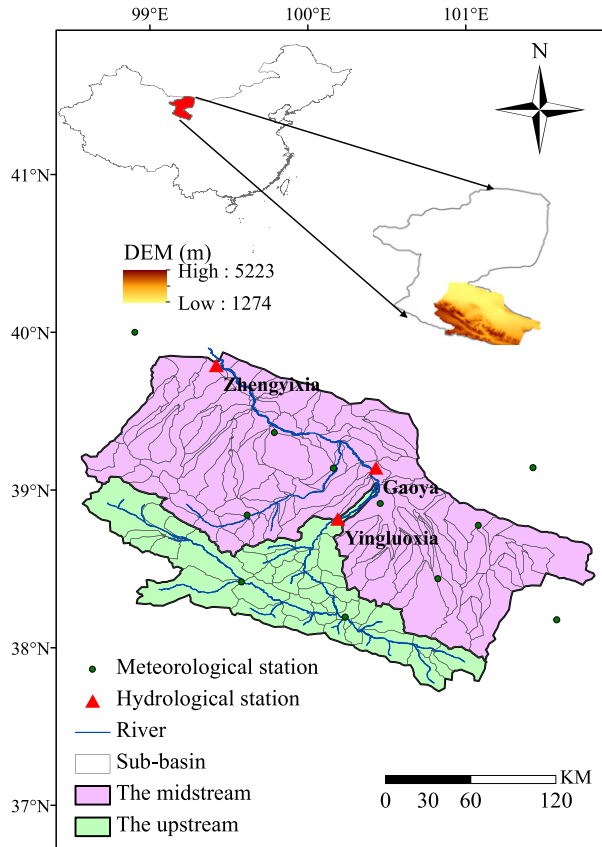


FIG. 1. Location of the upstream and midstream of the Heihe River basin and the geographic distribution of hydrometeorological stations.

provided by CMA. Monthly streamflow records of Yingluoxia (YLX) and Zhengyixia (ZYX) hydrological stations located at the outlet of the upstream and midstream of the HRB during 1961–2015 were provided by the Heihe Water Resources Department. In this study, upstream catchment average rainfall, temperature, and streamflow at YLX were used to characterize the climate and hydrology for the upstream; midstream catchment average rainfall and temperature and the difference of streamflow between ZYX and YLX were used to describe the climate and hydrology for the midstream. In addition, monthly streamflow data from Gaoya (GY; 1981–2000) station, which is located in the MHRB (Fig. 1), were also used to calibrate the hydrological model [see section 3d(2)].

3. Methodology

a. Drought characteristics analysis

In this study, SPI and SSI were used to characterize meteorological and hydrological droughts, respectively.

First, a probability distribution was fitted to the historical monthly precipitation or streamflow data for each month. Here, we used the empirical Gringorten plotting position (Farahmand and AghaKouchak 2015; Gringorten 1963) to generate the nonparametric standardized index:

$$p(x_i) = \frac{i - 0.44}{m + 0.12}, \quad (1)$$

where m is the length of time series for each month, i represents the rank of precipitation or streamflow data starting from the smallest, and $p(x_i)$ is the corresponding empirical probability. Then, the probability distribution was transformed to the standard normal distribution, which makes the standardized index comparable over time and space. We calculated the SPI and SSI at various time scales (SPI- n and SSI- n), which correspond to n -month precipitation and streamflow accumulation periods.

Drought events were defined as periods when the SPI (or SSI) value is consecutively below a given threshold (Fig. 2). If there is only 1 month or less between two drought events, and the SPI (or SSI) value of that month was still negative but greater than the given threshold, then the two events were then merged into one. Thresholds of -1 , -1.5 , and -2 were used to identify moderate, severe, and extreme drought events, respectively. These thresholds represent the probability of 10%, 5%, and 2% for SPI (or SSI) values to be lower than the corresponding thresholds. The number of event, duration, and severity were calculated for each catchment (upstream and midstream) at different accumulation periods and thresholds. The number of event was the total amount of all individual drought events. The duration was the constituent months of each drought event, and the severity was calculated by dividing the summation of SPI (or SSI) values by the duration for each individual event.

b. Drought propagation analysis

In this study, SPI and SSI were used to represent the meteorological and hydrological conditions, respectively. Therefore, the linkage between SPI and SSI can provide some indication of propagation from meteorological drought to hydrological drought through various hydrological processes. To investigate the appropriate propagation time from meteorological to hydrological drought, the correlations between SPI- n (n -month SPI) and SSI-1 (1-month SSI) time series were calculated. In the calculation of correlation coefficient, dry conditions are extracted from SPI- n and SSI-1 time series with SPI values less than zero. The period of SPI with the strongest correlation is considered as the most appropriate propagation time.

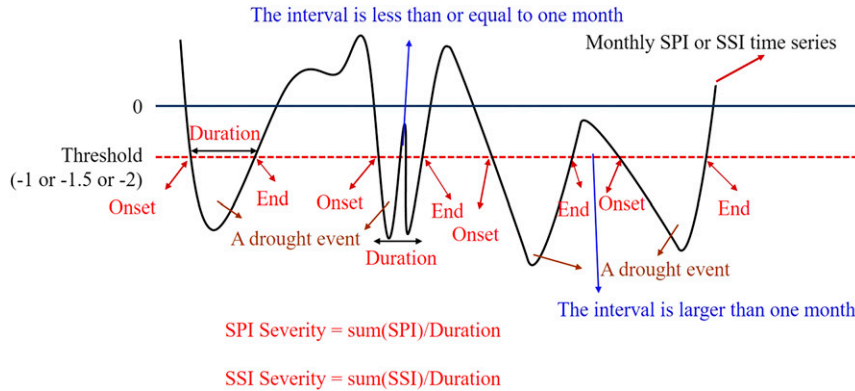


FIG. 2. Illustration of the identification of drought events and characteristics.

The SSI-1 was used considering its good description of short-term hydrological drought, similar to the 30-day mean flow (e.g., Gustard et al. 1992), and has been widely used for the drought propagation (e.g., Barker et al. 2016; Huang et al. 2017; Wu et al. 2016; Yuan et al. 2017).

In addition, the cross-wavelet transform (XWT; Grinsted et al. 2004) was used in this study to reveal the detailed correlations between SPI and SSI in both time and frequency domains. It is a new technique based on cross-spectrum analysis and wavelet transform, which can uncover the high common power and phase relationship between the two series. For two given time series x_n and y_n , the XWT is defined as $W^{xy} = W^x W^{y*}$, where $*$ refers to complex conjugation. Then the cross-wavelet power and relative phase are $|W^{xy}|$ and complex argument $\arg(W^{xy})$, respectively. Finally, the theoretical distribution of $|W^{xy}|$ with background power spectra P_k^x and P_k^y are calculated following Torrence and Compo (1998):

$$D \left[\frac{W_n^x(s) W_n^{y*}(s)}{\sigma_x \sigma_y} < p \right] = \frac{Z_v(p)}{v} \sqrt{P_k^x P_k^y}, \quad (2)$$

where $Z_v(p)$ is the confidence level connected with the probability p for probability distribution function, which is defined by the square root of two χ^2 distributions; v is 1 for real and 2 for complex wavelet.

c. Framework for separating effects of climate change and human activities

In the HRB, changes in hydrological processes are likely due to both climate change and human activities, which is reflected in the observed streamflow series Q_{obs} . Here, human activities refer to human water management including irrigation, reservoir regulation, domestic water, and industrial water use. The Heihe River basin has experienced an upward trend in both temperature and precipitation during 1961–2013 (Figs. 3c,d). We

designed three hydrological modeling experiments to distinguish contributions to hydrological drought from climate change and human activities. For this purpose, the Distributed Time-Variant Gain Hydrological Model (DTVGM; Xia et al. 2005a,b) was adopted and has been well calibrated (see section 3d). The first experiment was a control run, where the hydrological model was run with human activity modules turned on and driven by observed meteorological forcing. The simulated streamflow series Q_{Control} from the control run could reasonably represent actual hydrological conditions affected by both climate change and human activities, via model calibration [see section 3d(2)]. In the second experiment, scenario A, the naturalized streamflow series Q_A were reconstructed with the hydrological model. The model configuration is the same as in the control run except that the human activities modules were turned off in scenario A. In the third experiment, scenario B, the hydrological model with human activities modules turned off was driven by trend-removed meteorological forcing to reconstruct streamflow series Q_B without effects of climate change and human activities. In fact, some researchers have used climate model archives to account for climate change impacts (e.g., Williams et al. 2015). However, many climate models (e.g., CMIP5) have large errors in simulating precipitation and temperature (Zhao et al. 2017). Here, the trend-removed meteorological forcing was obtained by removing the annual trend from daily precipitation and temperature time series for each subbasin (Figs. 3c,d). The exact changes in temperature and precipitation on a day-to-day basis due to climate change are hard to quantify and are unlikely to be linear. To investigate the impact of such long-term trends in temperature and precipitation, we have to make some simple assumptions. We assumed that changes in temperature and precipitation could be represented by the annual trends of precipitation and temperature. Therefore, the difference between control run and scenario A is

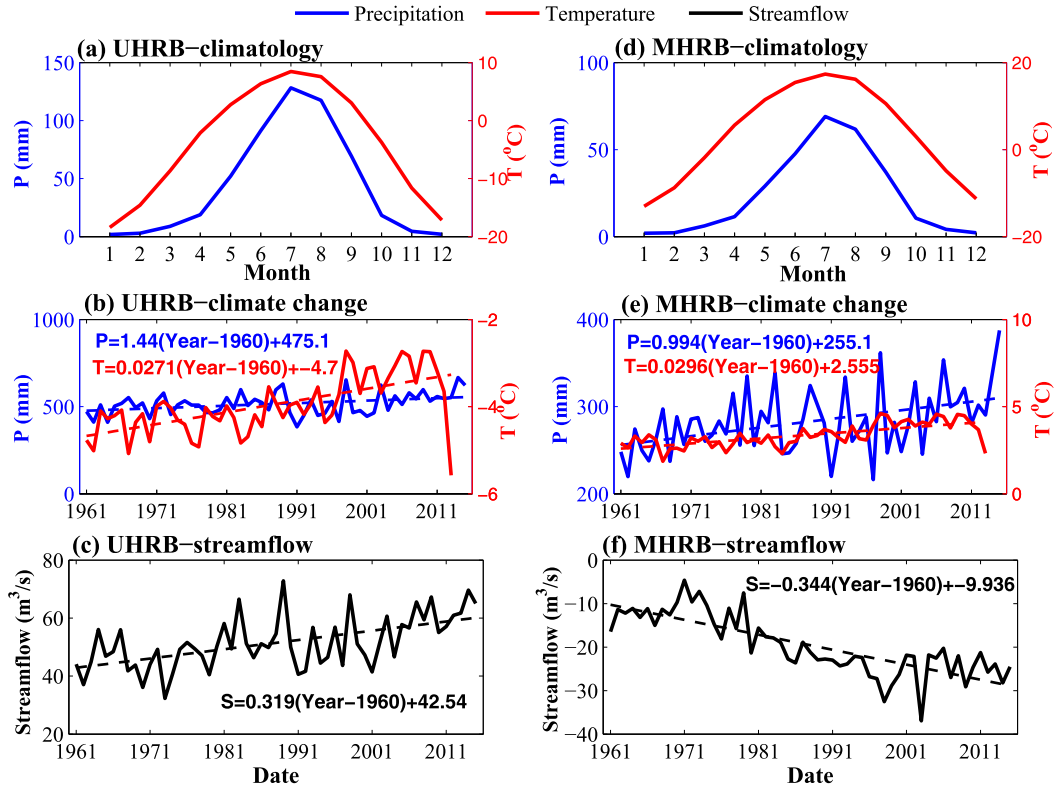


FIG. 3. The climatology and trend of precipitation, mean temperature, and streamflow in the (a)–(c) UHRB and (d)–(f) MHRB.

attributed to the human activities, and the difference between scenario A and scenario B can be attributed to long-term climate change. The comparison between the three model experiments could properly reduce some impacts from hydrological model structural errors.

Finally, the relative contributions of climate change η_C and human activities η_h to hydrological changes were calculated as

$$\Delta Q_h = Q_{\text{Control}} - Q_A, \quad (3)$$

$$\Delta Q_C = Q_A - Q_B, \quad (4)$$

$$\eta_h = \frac{\Delta Q_h}{|\Delta Q_h| + |\Delta Q_C|} \times 100\%,$$

$$\eta_C = \frac{\Delta Q_C}{|\Delta Q_h| + |\Delta Q_C|} \times 100\%. \quad (5)$$

d. A brief description of the DTVGM

The DTVGM was chosen for hydrological modeling and has been applied to many water-resource-related studies, such as separating naturalized and human-induced hydrology changes (Ma et al. 2014; Wang et al. 2009) and drought prediction (Ma et al. 2017). The

runoff model of DTVGM is based on a water balance function:

$$P_i + AW_i = AW_{i+1} + g_1 \left(\frac{AW_{ui}}{WM_u C_j} \right)^{g_2} P_i + AW_{ui} K_r + EP_i K_e + AW_{gi} K_g, \quad (6)$$

where i is the time period; j is subbasin number; P is precipitation (mm); AW_i and AW_{i+1} are the soil moisture (mm) at i and $i + 1$ moment; AW_u and AW_g are the upper and lower soil moisture (mm); WM_u is the upper saturated soil moisture (mm); C is the land cover parameter; and EP is potential evapotranspiration, which is calculated using air temperature based on the Hargreaves–Samani method (Hargreaves and Samani 1985). Coefficients in Eq. (6) are model parameters for calibration, including the soil permeability coefficient f_c ($0 - 30 \text{ mm h}^{-1}$), the runoff coefficient when the soil is saturated ($0 < g_1 < 1$), the soil moisture parameter ($g_2 > 0$), the subsurface runoff coefficient ($0 < K_r < 1$), the groundwater runoff coefficient ($0 < K_g < 1$), and the evapotranspiration coefficient ($0 < K_e < 1$). Another parameter for calibration is the Manning roughness coefficient n ($0.001 < n < 0.15$; Huggins and Monke 1966) in a routing model based on a kinematic

wave scheme. Considering abundant snow in the UHRB as a source of streamflow, the snowmelt module is integrated in the DTVGM. Snowmelt is calculated based on the degree-day factor (DDF) method (Li and Wang 2008). The detailed snowmelt process in the DTVGM can be found in Ye et al. (2010) and Ye et al. (2017).

1) HUMAN ACTIVITIES MODULES

In this study, reservoir module and water-use module are added into the DTVGM considering the actual hydrological processes in the HRB. In the DTVGM, for simplicity and practicality, one reservoir is constructed in each subbasin in the model. Its storage capacity is defined by summing all storage capacity values of all reservoirs in the actual subbasin. When there is no actual reservoir, the storage capacity is simply set to zero. Reservoir operation occurs after the subbasin routing, and the operating rule in the DTVGM has been described in Mao et al. (2016) and Xia et al. (2005a). In this study, the flood season refers to June–September, considering the climate in the UHRB and MHRB (Figs. 3a,b). The water-use module in the DTVGM primarily considers three types of water use: irrigation water, industrial water, and domestic water. The irrigation water is decided by irrigation area and irrigation quota. The irrigation area was calculated from a land-use dataset. The calculation of irrigation quota can be found in Mao et al. (2016). In the DTVGM, the industrial water use is the function of industrial gross domestic product (GDP), and the domestic water use is based on the population distribution. The detailed description and operating rule of both the reservoir and water-use modules in the DTVGM have been introduced by Mao et al. (2016), which has confirmed that the DTVGM could reasonably simulate water quantity in China. Here, the parameters in reservoir and water-use modules are estimated according to the observed datasets (Table 1). For example, in the reservoir module, the parameters, including dead water level, flood control water level, flow of full generating electricity, and minimum flow for ecological needs in both flood season and nonflood season, are set according to the realistic reservoir scheduling. In the water-use module, the irrigation quota, industrial water-use quota, and domestic water-use quota are determined by irrigation schedule and actual water use per unit GDP and per person, respectively. In this study, the reservoir module and water-use module are collectively known as human activities modules.

2) MODEL SETUP, CALIBRATION, AND VALIDATION

The upstream and midstream of the Heihe River basin were divided into 140 subbasins. All datasets for the model setup and calibration are presented in Tables 1 and 2, including meteorological forcings; GIS, agricultural,

TABLE 1. The detail information of dataset for the DTVGM.

Category	Data	Spatial scale	Temporal scale	Source	Reference
GIS	DEM Land use	90 m × 90 m 1:100 000	None In 2000	Data Center for Resources and Environmental Sciences, Chinese Academy of Sciences	http://srtm.csi.cgiar.org/ Liu and Buhe (2000); Tian et al. (2005)
Economy	Soil GDP Population	30 arc s 1 km × 1 km 1 km × 1 km	None None None		Shangguan et al. (2013) Liu et al. (2005) Mao et al. (2012)
Meteorology	Precipitation Maximum, mean, and minimum temperature	0.5° × 0.5° lon/lat 11 stations	Daily (1961–2013) Daily (1961–2013)	China Meteorological Administration	Zhao and Zhu (2015) None
Hydrology	Streamflow	3 stations	Monthly (Table 2)	Heihe Water Resources Department	None
Agricultural management	Irrigation water use	24 irrigation districts	Average monthly	Water Resources Bulletin, Statistical Yearbooks, and Irrigation annual report	None
Water projects	Total, flood regulation, flood control, utilizable, dead storage capacity	58 reservoirs	None	Cold and Arid Regions Sciences Data Center	http://westdc.westgis.ac.cn/ Zhang (2008)

TABLE 2. Performance of the DTVGM during calibration and validation periods at monthly scale.

	Calibration period	Validation period	Calibration period				Validation period			
			NSE	<i>R</i>	Bias	RMSE	NSE	<i>R</i>	Bias	RMSE
Y LX	1990–95	1996–2000	0.86	0.93	0.64	15.15	0.91	0.96	0.90	14.08
GY	1981–90	1991–2000	0.70	0.89	2.62	14.99	0.52	0.80	6.22	14.82
ZYX	1981–90	1991–2000	0.81	0.90	1.22	12.14	0.62	0.80	1.95	13.32

and eco-economic data; and hydrological data. The daily precipitation at 0.5° latitude–longitude grids and temperature at 11 meteorological stations were interpolated into each subbasin using the inverse distance weighting method, considering elevation correction for temperature. The GIS, agricultural, and economic data (e.g., land use, soil, GDP, population) were calculated for each subbasin based on the area percentage. The dynamic land use changed mainly in agricultural land change in the midstream, exhibiting a decreasing trend in the 1960s, an increasing trend in the 1970s (Chang et al. 2005), a decreasing trend during 1981–2006 (Zhang 2009), and an increasing trend during 2005–15 (increased by 3.37%). In this study, to simplify the hydrology model, we use a static land use (year of 2000) as the long-term average value. That may lead to some uncertainties, which can be reduced by adjusting the irrigation quota according to observed irrigation water.

First, we calibrated the DTVGM with human activities modules turned on using observed streamflow at Y LX, GY, and ZYX hydrological stations (Fig. 1). The Nash–Sutcliffe efficiency coefficient (NSE) and correlation coefficient *R* were used to assess the reliability of the model simulation. The accuracy measures at the monthly scale were $0.52 < \text{NSE} < 0.91$ and $0.8 < R < 0.96$ for both calibration and validation periods (Table 2). The comparisons between observation and simulation are also shown in Fig. 4. At the ZYX station, the mean difference between control run and scenario A (indicating the impact of human activities) is $52.29 \text{ m}^3 \text{ s}^{-1}$, much greater than the RMSE value (Table 2). The mean difference between scenarios A and B (indicating the impact of climate change) is $18.44 \text{ m}^3 \text{ s}^{-1}$, greater than the RMSE value (Table 2). Therefore, the human activities modules are reasonable to separate the influence of climate change and human activities, in spite of some uncertainties in the hydrology model. This indicated that the DTVGM performed well in simulating the hydrological processes over the HRB, especially for the upstream region.

4. Results and discussion

a. Drought characteristics

Time series of SPI and SSI for different time scales in the upstream and midstream of HRB are shown in

Fig. 5. In general, the climates in the upstream and midstream of HRB were getting wetter, while the hydrological conditions are more complex due to other factors at play, such as human activities, especially in the midstream region. As the time-scale increases, the time series of SPI and SSI become smoother with more prolonged wet and dry periods. In the upstream (Figs. 5a,b), the overall patterns of SPI and SSI time series are similar, with more dry episodes before 2007 while more wet episodes afterward. However, in the midstream (Figs. 5c,d), SPI and SSI time series appear to be quite different. For SPI (Fig. 5c), the variations are very similar to that in the upstream (Fig. 5a). But for SSI, there are more dry episodes in the later part of the record, especially after the 1980s (Fig. 5d).

For each catchment, drought events were identified based on thresholds of -1 , -1.5 , and -2 for both indices, and were characterized by the number of events, their duration, and severity. The numbers of meteorological and hydrological drought events are shown in Table 3. For shorter time scales (e.g., 1 and 6 months) and lower thresholds (i.e., -1 and -1.5), the number of meteorological droughts is far more than that of hydrological droughts in the upstream. As the accumulation period and threshold increase (i.e., more negative), the number of both meteorological and hydrological drought events decrease, which approach similar amounts of low values. However, in the midstream, there is no significant decrease in the number of hydrological drought events, compared with that of meteorological drought.

Figure 6 shows the preferred times for drought initiation and end (Figs. 6a,d), duration (Figs. 6e,f), and severity (Figs. 6g,h) for both meteorological and hydrological droughts and for both the UHRB and MHRB, at 1- and 6-month time scales using two drought thresholds. We examine the 1-month time scale (Fig. 6, top row) first. In the UHRB, for the lower threshold level (i.e., -1), the onset and end of drought mainly occurred between May and September (Figs. 6a,c), when more precipitation occurred but higher temperature, and therefore higher evapotranspiration, existed. The duration for hydrological droughts is longer than that for meteorological droughts (Fig. 6e). The drought

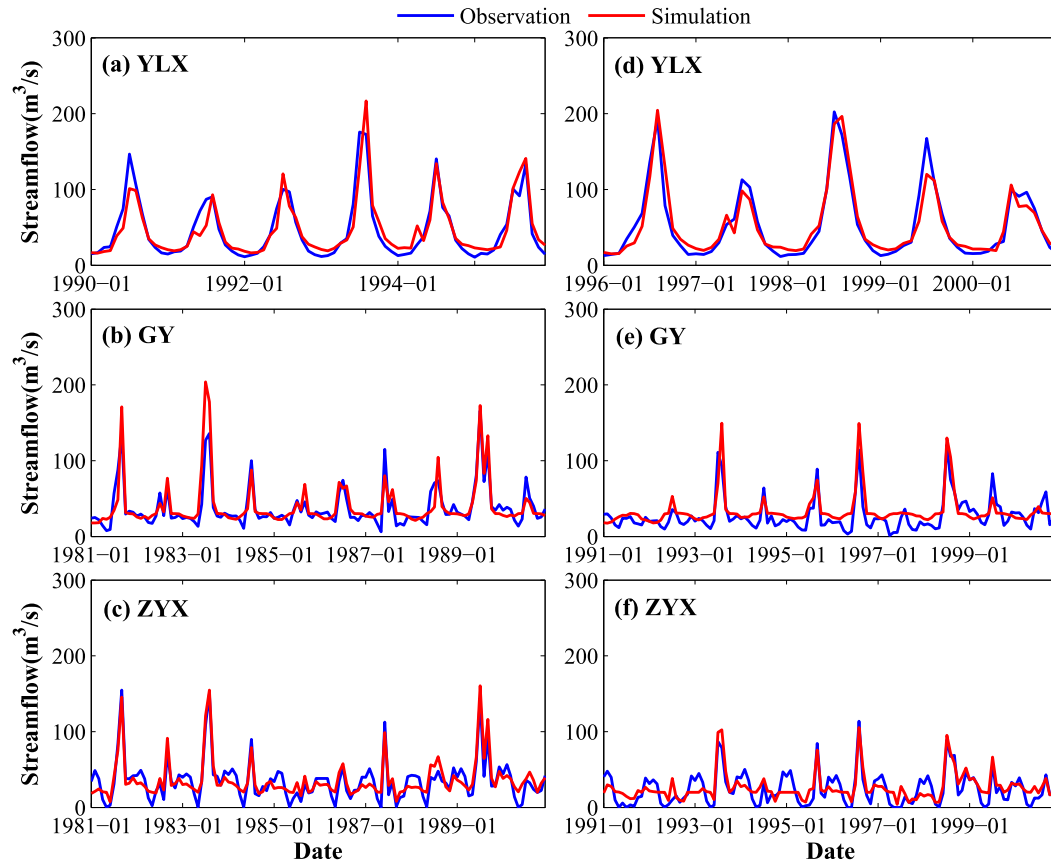


FIG. 4. Streamflow curve of the three hydrological stations during the (a)–(c) calibration period and (d)–(f) validation period.

severity shows no significant variations between meteorological and hydrological droughts (Fig. 6g). For the greater threshold (i.e., -1.5), the differences between meteorological and hydrological characteristics (i.e., timing, duration, and severity) are similar as that for the lower threshold.

In the MHRB, little difference exists between meteorological and hydrological drought characteristics. For the lower threshold, more droughts always happen between May and September (Figs. 6a,c), which are more likely due to lots of irrigation water in the midstream being needed during this period, in addition to higher evapotranspiration. In fact, the irrigation water requirements and evaporation presented a significant increasing trend from mid-May and peaked in late August and then decreased since early September (Tan and Zheng 2017). The duration of hydrological droughts shows little difference compared with that of meteorological droughts (Fig. 6e). Similarly, the meteorological and hydrological drought severity also shows little difference. In addition, the difference between meteorological and hydrological drought

characteristics basically stays the same for the two different thresholds.

For the 6-month time scale (Fig. 6, bottom row), most differences between meteorological and hydrological drought characteristics are similar to those at the 1-month scale. However, as the threshold level increases (i.e., from -1 to -1.5), the differences between durations for meteorological and hydrological droughts are more pronounced in the upstream. In the midstream, the hydrological drought durations are slightly longer than meteorological droughts, less than the difference in the upstream (Fig. 6f). For the greater threshold, the hydrological drought severity is more concentrated than meteorological droughts (Fig. 6h). That is likely due to human activities that play a more important role in water resource use in the midstream of HRB (Deng and Zhao 2015; Sun et al. 2016).

b. Drought propagation

The correlations between SSI-1 and SPI- n (1–12 months) on dry conditions for each catchment are shown in Fig. 7. The relationship between meteorological and

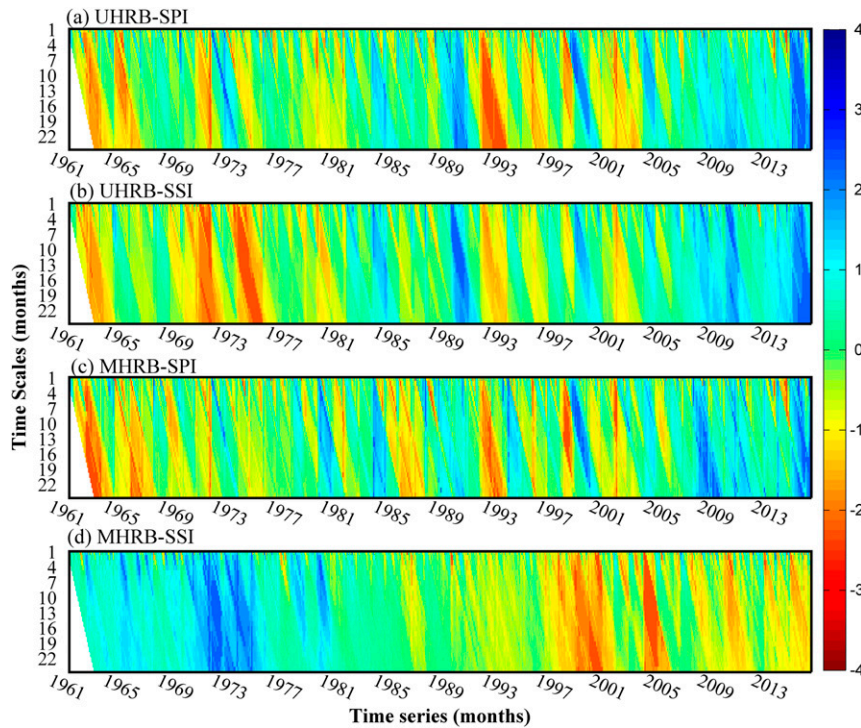


FIG. 5. Time series of monthly SPI and SSI at different accumulation periods in the (a),(b) UHRB and (c),(d) MHRB. For each panel, the y axis represents the different accumulation periods (1–24 months), and the x axis is the time in months (1961–2015).

hydrological droughts and propagation behaviors shows significant seasonal variations and regional differences. In the upstream (Fig. 7a), the correlations are higher in May–October than in cold seasons, when

TABLE 3. Number of meteorological and hydrological drought events identified by SPI and SSI series during 1961–2015.

Threshold	Time scales (months)	No. of events		
		UHRB	MHRB	
SPI	-1	1	80	78
		6	38	36
		18	12	19
	-1.5	1	40	41
		6	18	20
		18	9	11
	-2	1	11	11
		6	9	9
		18	2	5
SSI	-1	1	44	72
		6	22	24
		18	9	9
	-1.5	1	21	38
		6	8	13
		18	6	3
	-2	1	9	11
		6	2	3
		18	2	3

stronger correlations exist at longer SPI accumulation periods. The propagation time (i.e., the strongest correlation) from meteorological drought to hydrological drought was the shortest in February–March and September–October (1–3 months), followed by April–June, August, and November–December (6–10 months), and was longest in January and July (11–12 months). The shortest propagation time in February–March is likely related to less antecedent precipitation, most of which are landing as snow during the cold season. During September–October, strong evapotranspiration due to higher temperatures during the antecedent warm season (e.g., July–August) that tightly links rainfall and streamflow variations, combined with less precipitation, lead to less streamflow storage and thus short propagation time from precipitation deficit to hydrological drought. Longer propagation time in April–June is probably associated with the melting of snow and glaciers in the Qilian Mountains when temperature is rising, which disconnects the precipitation variation with streamflow variation as melting contributes water in the streams. In July–August, most precipitation occurs (Fig. 3a) and abundant streamflow storage has been generated by snowmelt, leading to longer propagation time. During the cold seasons (e.g., November–January), weak evapotranspiration due to lower temperature results in longer

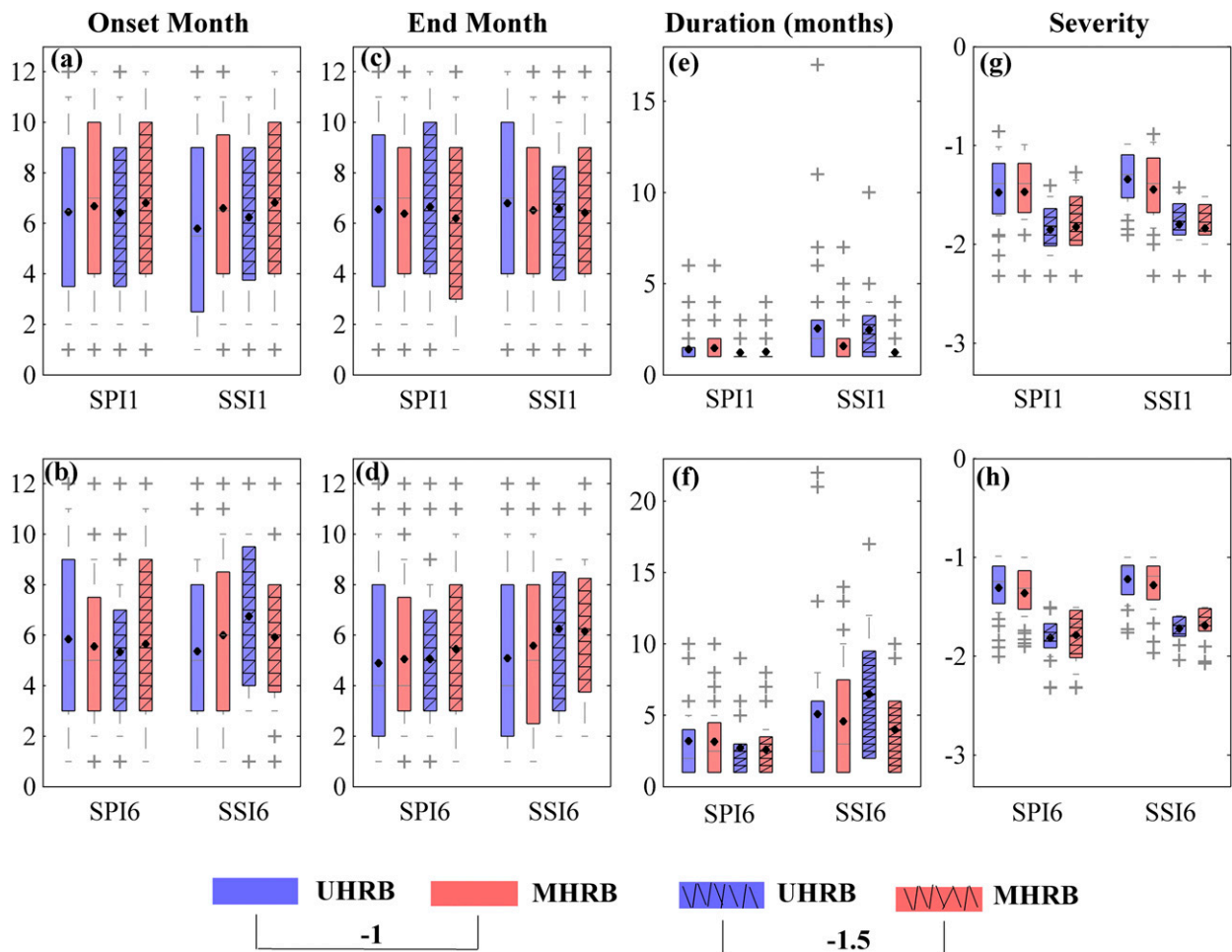


FIG. 6. Box plots showing meteorological and hydrological drought characteristics based on SPI-1, SPI-6, SSI-1, and SSI-6 using thresholds of -1 and -1.5 for the UHRB and MHRB. The blue boxes represent characteristics in the upstream, and the red boxes represent characteristics in the midstream. The boxes without and with black oblique lines are characteristics using thresholds of -1 and -1.5 , respectively. The black rhombus in each box represents the mean value.

propagation time from meteorological drought to hydrological drought.

In the midstream (Fig. 7b), the correlations between SSI-1 and SPI- n are lower than those in the upstream, indicating a weaker relationship between meteorological and hydrological drought and suggesting that other factors are at play shaping the hydrological processes in the midstream. During the warm seasons (April–August), the correlation even turns negative. The midstream has the major urban area and large farmlands with irrigated agriculture. Even in years with above-normal precipitation in the region, streamflow can still be low as water is used for irrigation in the semiarid region and for filling the surface reservoirs in addition to the strong loss to evapotranspiration. The negative correlation between precipitation and streamflow is evidence of how human water use and management can

disrupt the natural hydrological cycle. Under such an influence, the propagation time from meteorological to hydrological drought can vary substantially between seasons and differ from that in the upstream. The shortest propagation time happens in October–January (1–4 months), which may be attributed to the reservoir filling during flood season (June–September), vast irrigation water for crops during irrigation season (April–September; Akiyama 2009; Tan and Zheng 2017), and less precipitation and less inflow from the UHRB due to freezing in October–January, which leads to low flow. In addition, the correlations between longer time scales of SSI- n (e.g., SSI-3, SSI-6, and SSI-12) and SPI- n are shown in the appendix (Fig. A1).

Furthermore, to investigate the detailed linkage between meteorological and hydrological drought, the XWT was applied in this study. Figure 8 shows the XWT

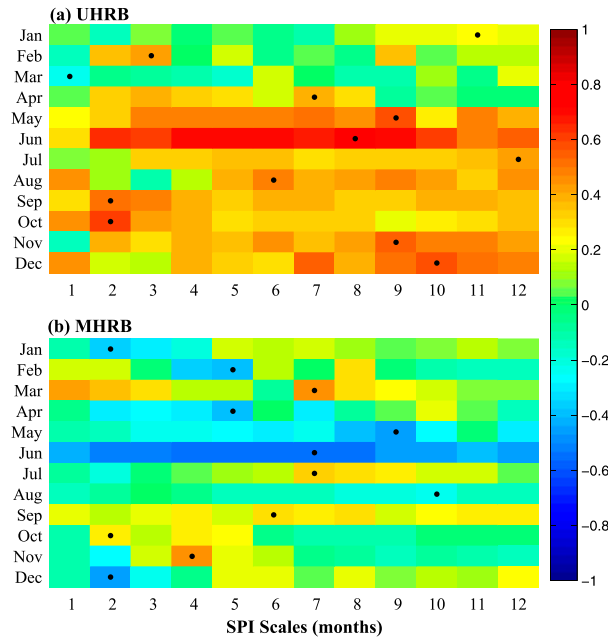


FIG. 7. The correlation coefficients between SSI-1 and SPI-*n* on dry conditions for observation, in the (a) UHRB and (b) MHRB. Here, dry conditions are extracted from SPI-*n* and SSI-1 series with SPI values less than zero. The *x* axis is the various time scales of SPI (1, . . . , 12 months), and the *y* axis is the different months at the intra-annual scale. The color represents the correlation coefficients between SSI-1 and SPI-*n* series, with deep red and blue colors denoting high and low correlation coefficients, respectively. Significant correlations ($p < 0.05$) correspond to correlation coefficient values larger than 0.37. Note that the black dot denotes the strongest correlation for the period of 1961–2015.

results for the SPI-1 and SSI-1 time series in October–February (dry seasons), March–May (snowmelt seasons), and June–September (rainy seasons) in the upstream and midstream. Note that in Fig. 8, the color refers to cross-wavelet power at that time–frequency space. Higher values represent higher common power between two variables, which is exhibited as a thick contour using the 5% confidence level against red noise. The arrows in Fig. 8 denote the relative phase relationship, with positive correlations pointing to the right, and negative associations pointing to the left. The relationships between SPI-1 and SSI-1 in the upstream are mainly positive (Figs. 8a–c). The correlations are more apparent during rainy seasons, and less significant during snowmelt seasons. In the midstream (Figs. 8d–f), there are no significant positive correlations between meteorological and hydrological droughts, especially during snowmelt and rainy seasons (i.e., irrigation seasons). The analysis has further confirmed the relationship between meteorological drought and hydrological drought in the upstream and midstream presented in earlier sections.

c. Separating natural and human-induced hydrological droughts

Besides climate, human activities can also modify the hydrological processes underlying drought propagation (Van Loon et al. 2016). Figure 9 displays the differences between simulated SSI-1 time series from the control run and scenarios A and B in the upstream and midstream of HRB. It can be observed that climate change, especially the long-term upward trends in precipitation, helps to increasing SSI values, thus reducing hydrological drought (Figs. 9c,d). In the upstream (Fig. 9a), human activities have little effect on hydrological drought alleviation and aggravation. In the midstream (Fig. 9b), human activities have substantially alternated hydrological drought throughout the entire study period, and aggravated more hydrological droughts since 2000s, due to more water consumption for agricultural purposes (Fig. 3f; Lu et al. 2015; Li et al. 2017).

Tables 4 and 5 summarize the hydrological drought characteristics in the upstream and midstream from observation and different scenarios. The DTVGM underestimated the number of hydrological drought events and overestimated the mean duration and severity. In the upstream (Table 4), the differences in the number of drought events, mean duration, and severity between the control run and scenarios A and B are small, indicating that both climate change and human activities have little impact on hydrological drought characteristics. In the midstream (Table 5), there are larger differences of number of events and duration between the control run and scenario A, indicating that human activities have greater impacts on hydrological drought. Human activities have increased the number of hydrological drought events and mean severity, but have reduced drought duration. In fact, human activities, such as reservoir operations and artificial channels for water delivery, could also play an active role in drought alleviation (Lu et al. 2015; Xi et al. 2010).

Figure 10 displays the correlations between SPI-*n* and SSI-1 on dry conditions for control run and scenarios A and B. In the upstream (Figs. 10a,c,e), the impacts of climate change and human activities on the correlation and drought propagation behaviors are small. Climate change has slightly increased propagation time in September and decreased propagation time in January and August (Figs. 10c,e). Climate warming has led to increasing temperature and precipitation (Fig. 3d) and more snowmelt for easing hydrological dry conditions. However, higher temperature also caused stronger evapotranspiration, which accelerates hydrological drought much easier. Human activities have increased the propagation time in January–February but decreased propagation time in

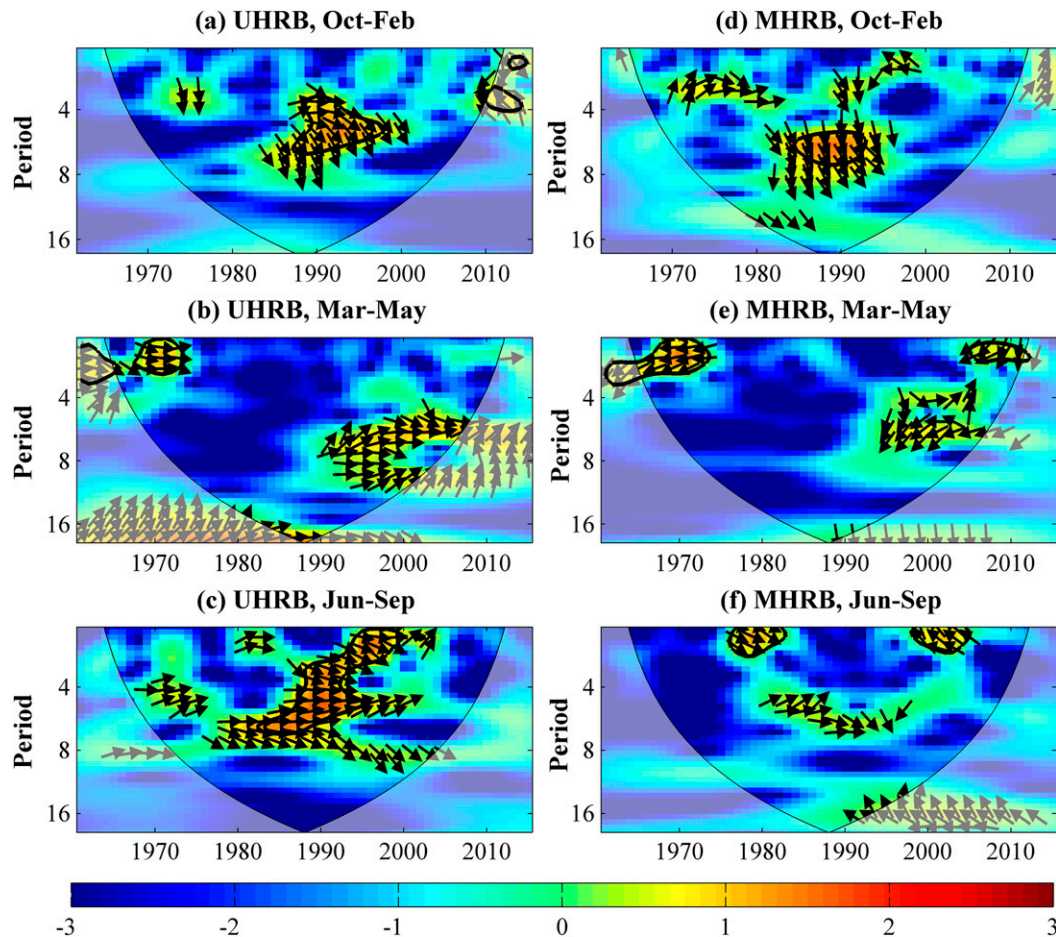


FIG. 8. Cross-wavelet transform for SPI-1 and SSI-1 in October–February, March–May, and June–September in the (a)–(c) UHRB and (d)–(f) MHRB. Note that thick contours denote 5% significance levels against red noise. The relative phase relationship is denoted as arrows (positive correlation, arrows point right; negative correlation, arrows point left). The “U” shaped line refers to the cone of influence.

September (Figs. 10a,c). That may be attributed to the reservoir operation. In the MHRB (Figs. 10b,d,f), human activities have a greater effect than climate change, which has slightly increased the propagation time in cold seasons (March and October–December) but decreased propagation time in January, June, and September. It can be observed that the correlations were significantly increased when human activities were removed, especially during April–November in the midstream (Figs. 10b,d). This means that human activities have distinctly modified the relationship between precipitation and streamflow, which made the hydrological processes more complex. The effects of human activities are more pronounced in April–November, where crop growth and more irrigation happened. The propagation time was significantly reduced in September–November (Figs. 10b,d) due to larger water consumption for antecedent irrigation, which leads to less water storage in river channels.

In other seasons, for example, January, longer propagation time was detected likely due to regulated discharge in dry seasons.

To quantify the effects of climate change and human activities on hydrological processes, their contributions were estimated. Figure 11 shows the relative contributions of climate change and human activities on the mean state and variability of streamflow for the upstream and midstream of HRB. In the upstream, as mentioned above, the impacts of both climate change and human activities were small. Among them, climate change acts to decrease streamflow (Fig. 11a) and hydrological variability (Fig. 11c) before the 1980s, but has reversed since the 1990s. Human activities invariably play a role in decreasing streamflow (Fig. 11a), with the strongest effects during the 1980s and 1990s. In addition, human activities have increased hydrological variability in the upstream (Fig. 11c) by transporting more and

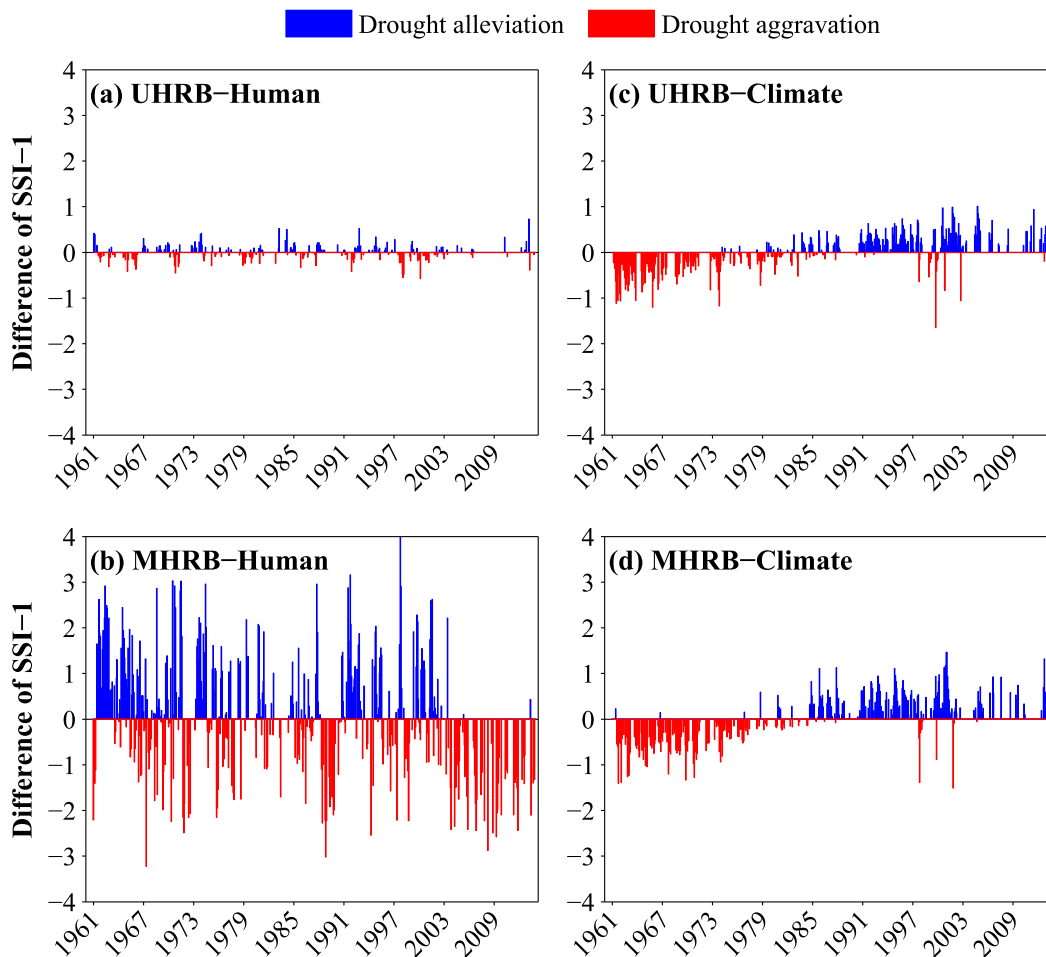


FIG. 9. (a),(b) The difference between simulated SSI-1 time series of control run and scenario A during 1961–2013 representing the impact of human activities on hydrological drought, and (c),(d) the difference between scenario A and scenario B representing the impact of climate change on hydrological drought, in the (top) UHRB and (bottom) MHRB.

more water into the midstream. In the midstream, the contributions of climate change and human activities on streamflow (Fig. 11b) were both negative, indicating a higher probability of hydrological droughts. Human activities were the predominant factor for hydrological drought, accounting for between -89% and -99% ,

while climate change only contributed less than 11% (less negative) during 1961–2013. Climate change has decreased the hydrological variability, while human activities play a more important role in increasing hydrological variability before the 2000s (Fig. 11d). However, hydrological variability has decreased since the 2000s (Fig. 11d), more likely due to human activities, such as more reservoirs, irrigation infrastructure, and water transfer projects (Lu et al. 2015). In general, climate change tended to increase the water resources, while hydrological droughts were more likely to occur because human activities were the major contribution factor for water consumption in the HRB.

TABLE 4. Hydrological drought characteristics for the observation and three scenarios using a threshold of -1 during 1961–2013 in the UHRB.

Period	No. of events	Duration (months)		Severity	
		Mean	Max	Mean	Max
Observation	44	2.55	17	-1.34	-1.91
Control run	34	3.03	15	-1.44	-2.31
Scenario A	37	2.70	15	-1.44	-2.31
Scenario B	35	2.86	11	-1.42	-2.31

d. Discussion

Human activities play both active and passive roles in hydrological processes in the HRB, via a large number of water conservancy projects, for example, reservoirs,

TABLE 5. Hydrological drought characteristics for the observation and three scenarios using a threshold of -1 during 1961–2013 in the MHRB.

Period	No. of events	Duration (months)		Severity	
		Mean	Max	Mean	Max
Observation	66	1.61	7	-1.43	-2.32
Control run	58	1.79	6	-1.50	-2.31
Scenario A	42	2.45	20	-1.49	-2.31
Scenario B	46	2.24	9	-1.47	-2.31

irrigation infrastructure, and water transfer projects. Water resources exploitation of the HRB is primarily developed for agricultural irrigation in the midstream

region through artificial canals and reservoir construction (Liu and Shen 2018; Wang and Gao 2002). Land use and land cover have changed dramatically since the 1950s, with increased farmland and water requirement amount, especially in the last 30 years (Hu et al. 2015; Lu et al. 2015; Liu and Shen 2018). However, the streamflow supplied to the downstream also showed a significant decrease since 1990 (Jia et al. 2011), with an increase of reservoirs (Wu et al. 2005). These increased the water resource stress and accelerated the occurrence of hydrological droughts. On the other hand, reservoir construction also altered the hydrological processes and the relationship between meteorological and hydrological droughts in the HRB. By 1994, 98 reservoirs were built, most of which were located in the midstream

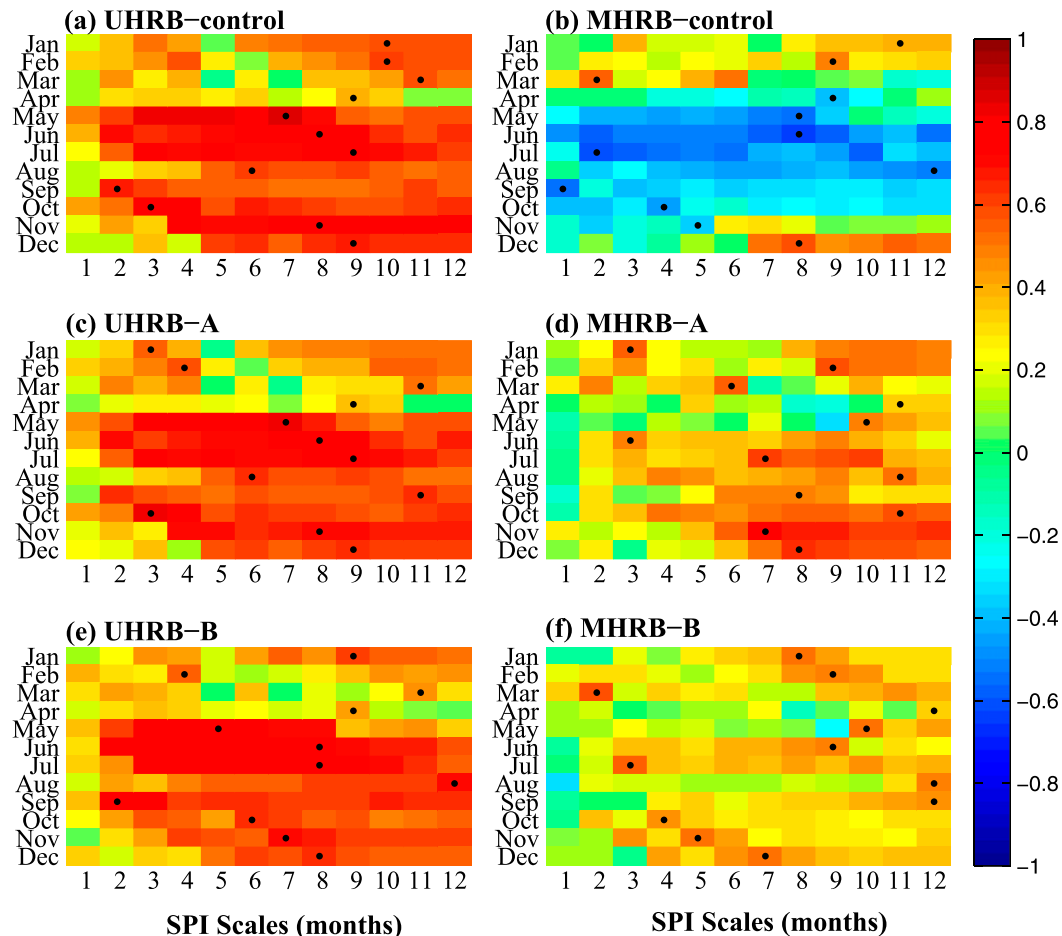


FIG. 10. The correlation coefficients between SSI-1 and SPI- n on dry conditions for (a),(b) the control run; (c),(d) scenario A; and (e),(f) scenario B in the (left) UHRB and (right) MHRB. Here, dry conditions are extracted from SPI- n and SSI-1 series with SPI values less than zero. The x axis is the various time scales of SPI (1, ..., 12 months), and the y axis is the different months at the intra-annual scale. The color represents the correlation coefficients between SSI-1 and SPI- n series, with deep red and blue colors denoting high and low correlation coefficients, respectively. Significant correlations ($p < 0.05$) correspond to correlation coefficient values larger than 0.37. Note that the black dot denotes the strongest correlation for the period of 1961–2013.

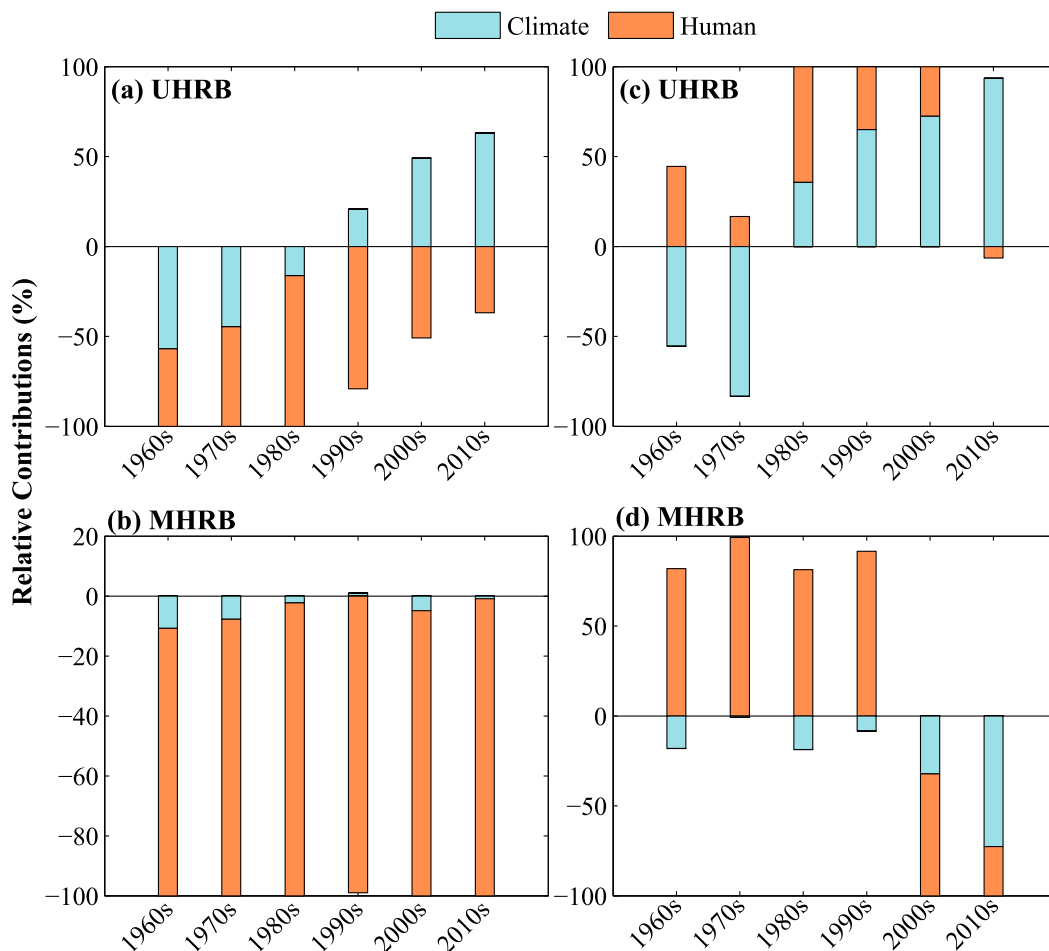


FIG. 11. Relative contributions of climate change and human activities on (a),(b) streamflow and (c),(d) hydrological variability in the UHRB and MHRB. Note that positive contribution means climate change or human activities lead to increasing streamflow or hydrologic variability, while negative contribution refers to decreasing streamflow or hydrologic variability.

region, and water storage capacity increased quickly (Wang and Gao 2002). The reservoirs can alleviate the severe and extreme droughts by releasing water that has been stored during the flood seasons to the streams during low-flow periods (Wan et al. 2017).

In this study, we designed three modeling experiments to distinguish the effects of climate change and human activities based on the assumption that model errors were small enough to simulate actual and natural streamflow series. The control run was performed with human activities modules turned on to obtain streamflow series similar to observations. Therefore, comparison between simulations could appropriately reduce some impacts from model structural errors. However, no model is perfect, and the findings here may have some model dependency. Therefore, there is a need to apply multiple hydrological models to reduce the uncertainties and verify the results of separation in a future study. Owing to the fact that natural

runoff free of human impact does not exist in this basin, the hydrological model was first calibrated using observed streamflow, and then run with removed human activities modules to simulate the naturalized streamflow series. In fact, there is much room for improvement. For instance, the human activities modules can be improved further. To better simulate human water management, the scheme involving irrigation water can be improved, considering the actual irrigation technology (e.g., sprinkler irrigation or flood irrigation, draw water from channel or groundwater). Higher-precision data involved in anthropogenic water withdrawal and use (e.g., irrigation amount related to the crop) should be continually developed.

5. Conclusions

This study analyzed the meteorological and hydrological drought characteristics and propagation behaviors in the

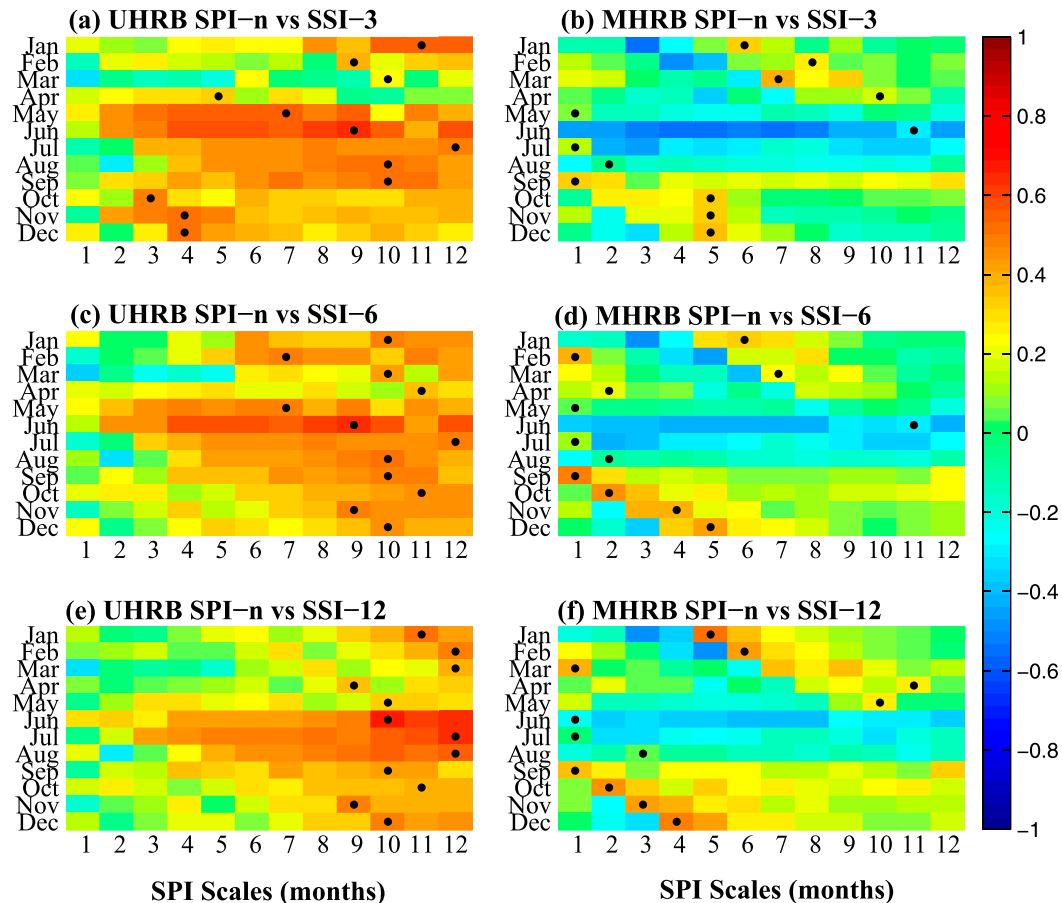


FIG. A1. The correlation coefficients between (a),(b) SSI-3; (c),(d) SSI-6; and (e),(f) SSI-12 and SPI- n on dry conditions for observation, in the (left) UHRB and (right) MHRB. Here, dry conditions are extracted from SPI- n and SSI- n series with SPI values less than zero. The x axis is the various time scales of SPI (1, ..., 12 months), and the y axis is the different months at the intra-annual scale. The color represents the correlation coefficients between SSI- n and SPI- n series, with deep red and blue colors denoting high and low correlation coefficients, respectively. Significant correlations ($p < 0.05$) correspond to correlation coefficient values larger than 0.37. Note that the black dot denotes the strongest correlation for the period of 1961–2015.

upstream and midstream of the Heihe River basin (HRB) using SPI and SSI at various time scales. The effects of climate change and human activities on hydrological drought were also explored. In the upstream, the overall dry/wet patterns of SPI and SSI series are similar, showing high positive correlations between meteorological and hydrological droughts, especially during warm and rainy seasons. Droughts were more likely to occur and terminate in May–August, where high evaporation but also more snowmelt and precipitation existed. When using a given threshold to identify drought, meteorological and hydrological drought characteristics show some differences. Drought events became much fewer and longer when moving from precipitation to streamflow storage. The propagation behaviors show significant seasonal variations, with shortest propagation time in February–March

and September–October (1–3 months). Both the impacts of climate change and human activities on hydrological droughts were relatively small, with more negative impacts from human activities especially during the 1980s and 1990s.

In the midstream, climate conditions showed a wetting trend, while hydrology conditions were more complex and showed a drying trend due to human activities. The meteorological drought characteristics are similar to those in the upstream, while more hydrological drought events were detected in the midstream. This is attributable to more human water management occurring in the midstream oases regions than in the upstream mountainous region (Qi and Luo 2005). The durations for meteorological and hydrological droughts are similar, with slightly longer durations for hydrological

droughts at longer time scales. The correlations between meteorological and hydrological droughts are lower and even negative in warm and irrigation seasons, due to vast water management systems (e.g., irrigation, reservoir regulation). Short propagation time was detected in October–January due to antecedent irrigation and less precipitation.

Compared with the effects from climate change, human activities play a dominant role in the occurrence of hydrological drought in the midstream, contributing between -89% and -99% . In addition, more hydrological drought events were extracted while drought duration and severity were decreased when human activities affected the hydrological cycle. It is not surprising to see that more human activities have reduced the propagation time from meteorological drought to hydrological drought, especially in the crop-growing seasons. Meanwhile, human activities have increased hydrological variability by water regulation via artificial canals and reservoir construction. These operations could work on relieving severe and extreme hydrological droughts, and thus shorten their durations.

In general, the understanding of drought characteristics and propagation processes provided by this study can be helpful for future development of drought warning systems for better drought preparedness.

Acknowledgments. This study was supported by the Natural Science Foundation of China (51879009, 41475093), the Strategic Priority Research Program of the Chinese Academy of Sciences (XDA19070104, XDA20060401), and the State Key Laboratory of Earth Surface Processes and Resource Ecology Open Research Program (2017-KF-17). This work is also supported by the Water Science Network WaterCube Program at Michigan State University. We thank the China Meteorological Administration (<http://data.cma.cn>) for making precipitation and temperature information available and hydrology bureau for providing streamflow data.

APPENDIX

The Relationship between SSI- n and SPI- n

Figure A1 shows the correlations between SSI- n at longer time scales (e.g., SSI-3, SSI-6, and SSI-12) and SPI- n (1–12 months). In the upstream (Figs. A1a,c,e), as the time scale of SSI increases, higher correlation is detected in longer accumulated periods of SPI. The propagation time increases when meteorological drought propagates into longer-term hydrological drought. However, in the midstream (Figs. A1b,d,f), few differences

are found between different time scales of SSI because human activities play an important role on drought propagation.

REFERENCES

- Akiyama, T., 2009: Accelerating human impacts on the water resources in the Heihe River basin, northwestern China. *ICCS J. Mod. Chin. Stud.*, **1**, 35–50.
- Barker, L. J., J. Hannaford, A. Chiverton, and C. Svensson, 2016: From meteorological to hydrological drought using standardised indicators. *Hydrol. Earth Syst. Sci.*, **20**, 2483–2505, <https://doi.org/10.5194/hess-20-2483-2016>.
- Chang, J., G. Wang, and Y. Wang, 2005: Driving factors of land use change in the Heihe River: Case study of Zhangye prefecture. *J. Glaciol. Geocryol.*, **27**, 117–123.
- Deng, X., and C. Zhao, 2015: Identification of water scarcity and providing solutions for adapting to climate changes in the Heihe River basin of China. *Adv. Meteor.*, **2015**, 279173, <https://doi.org/10.1155/2015/279173>.
- Eltahir, E. A. B., and P. J.-F. Yeh, 1999: On the asymmetric response of aquifer water level to floods and droughts in Illinois. *Water Resour. Res.*, **35**, 1199–1217, <https://doi.org/10.1029/1998WR900071>.
- Farahmand, A., and A. AghaKouchak, 2015: A generalized framework for deriving nonparametric standardized drought indicators. *Adv. Water Resour.*, **76**, 140–145, <https://doi.org/10.1016/j.advwatres.2014.11.012>.
- Gringorten, I. I., 1963: A plotting rule for extreme probability paper. *J. Geophys. Res.*, **68**, 813–814, <https://doi.org/10.1029/JZ068i003p00813>.
- Grinsted, A., J. C. Moore, and S. Jevrejeva, 2004: Application of the cross wavelet transform and wavelet coherence to geophysical time series. *Nonlinear Processes Geophys.*, **11**, 561–566, <https://doi.org/10.5194/npg-11-561-2004>.
- Gustard, A., A. Bullock, and J. M. Dixon, 1992: Low flow estimation in the United Kingdom. IH Rep. 108, 88 pp., http://nora.nerc.ac.uk/id/eprint/6050/1/IH_108.pdf.
- Hannaford, J., B. Lloyd-Hughes, C. Keef, S. Parry, and C. Prudhomme, 2011: Examining the large-scale spatial coherence of European drought using regional indicators of precipitation and streamflow deficit. *Hydrol. Processes*, **25**, 1146–1162, <https://doi.org/10.1002/hyp.7725>.
- Hargreaves, G. H., and A. Z. Samani, 1985: Reference crop evapotranspiration from temperature. *Appl. Eng. Agric.*, **1**, 96–99, <https://doi.org/10.13031/2013.26773>.
- Hu, X., L. Lu, X. Li, J. Wang, and M. Guo, 2015: Land use/cover change in the middle reaches of the Heihe River basin over 2000–2011 and its implications for sustainable water resource management. *PLOS ONE*, **10**, e0128960, <https://doi.org/10.1371/journal.pone.0128960>.
- Huang, S., P. Li, Q. Huang, G. Leng, B. Hou, and L. Ma, 2017: The propagation from meteorological to hydrological drought and its potential influence factors. *J. Hydrol.*, **547**, 184–195, <https://doi.org/10.1016/j.jhydrol.2017.01.041>.
- Huggins, L. F., and E. J. Monke, 1966: The mathematical simulation of the hydrology of small watersheds. IWRRC Tech. Rep. 1, 147 pp.
- Hutchinson, M. F., 1998a: Interpolation of rainfall data with Thin Plate Smoothing Splines - Part I: Two dimensional smoothing of data with short range correlation. *J. Geogr. Inf. Decis. Anal.*, **2** (2), 139–151.

- , 1998b: Interpolation of rainfall data with Thin Plate Smoothing Splines - Part II: analysis of topographic dependence. *J. Geogr. Inf. Decis. Anal.*, **2** (2), 152–167.
- Jia, L., H. Shang, G. Hu, and M. Menenti, 2011: Phenological response of vegetation to upstream river flow in the Heihe River basin by time series analysis of MODIS data. *Hydrol. Earth Syst. Sci.*, **15**, 1047–1064, <https://doi.org/10.5194/hess-15-1047-2011>.
- Li, H. Y., and J. Wang, 2008: The snowmelt runoff model applied in the upper Heihe River basin (in Chinese). *J. Glaciol. Geocryol.*, **5**, 769–775.
- Li, S., Y. Zhao, Y. Wei, and H. Zheng, 2017: Evolution of the vegetation system in the Heihe River basin in the last 2000 years. *Hydrol. Earth Syst. Sci.*, **21**, 4233–4244, <https://doi.org/10.5194/hess-21-4233-2017>.
- Li, X., L. Lu, G. D. Cheng, and H. L. Xiao, 2001: Quantifying landscape structure of the Heihe River Basin, north-west China using FRAGSTATS. *J. Arid Environ.*, **48**, 521–535, <https://doi.org/10.1006/jare.2000.0715>.
- Liu, B., W. Z. Zhao, X. X. Chang, S. B. Li, Z. H. Zhang, and M. W. Du, 2010: Water requirements and stability of oasis eco-system in arid region, China. *Environ. Earth Sci.*, **59**, 1235–1244, <https://doi.org/10.1007/s12665-009-0112-7>.
- Liu, H., and Coauthors, 2005: Spatialization approach to 1 km Grid GDP supported by remote sensing. *Geo-Inf. Sci.*, **7**, 120–123.
- Liu, J., and A. S. Buhe, 2000: Study on spatial-temporal feature of modern land-use change in China: Using remote sensing technique (in Chinese). *Quat. Sci.*, **3**, 229–239.
- Liu, X., and Y. Shen, 2018: Quantification of the impacts of climate change and human agricultural activities on oasis water requirements in an arid region: a case study of the Heihe River basin, China. *Earth Syst. Dyn.*, **9**, 211–225, <https://doi.org/10.5194/esd-9-211-2018>.
- Lu, Z., Y. Wei, H. Xiao, S. Zou, J. Xie, J. Ren, and A. Western, 2015: Evolution of the human–water relationships in the Heihe River basin in the past 2000 years. *Hydrol. Earth Syst. Sci.*, **19**, 2261–2273, <https://doi.org/10.5194/hess-19-2261-2015>.
- Ma, F., A. Ye, W. Gong, Y. Mao, C. Miao, and Z. Di, 2014: An estimate of human and natural contributions to flood changes of the Huai River. *Global Planet. Change*, **119**, 39–50, <https://doi.org/10.1016/j.gloplacha.2014.05.003>.
- , —, and Q. Duan, 2017: Seasonal drought ensemble predictions based on multiple climate models in the upper Han River Basin, China. *Climate Dyn.*, <https://doi.org/10.1007/s00382-017-3577-1>.
- Ma, M. G., and V. Frank, 2006: Interannual variability of vegetation cover in the Chinese Heihe River Basin and its relation to meteorological parameters. *Int. J. Remote Sens.*, **27**, 3473–3486, <https://doi.org/10.1080/01431160600593031>.
- Mao, Y., A. Ye, and J. Xu, 2012: Using land use data to estimate the population distribution of China in 2000. *GLSci. Remote Sens.*, **49**, 822–853, <https://doi.org/10.2747/1548-1603.49.6.822>.
- , —, X. Liu, F. Ma, X. Deng, and Z. Zhou, 2016: High-resolution simulation of the spatial pattern of water use in continental China. *Hydrol. Sci. J.*, **61**, 2626–2638, <https://doi.org/10.1080/02626667.2016.1153102>.
- Mishra, A. K., and V. P. Singh, 2010: A review of drought concepts. *J. Hydrol.*, **391**, 202–216, <https://doi.org/10.1016/j.jhydrol.2010.07.012>.
- Pan, X. D., X. Li, K. Yang, J. He, Y. L. Zhang, and X. J. Han, 2014: Comparison of downscaled precipitation data over a mountainous watershed: A case study in the Heihe River Basin. *J. Hydrometeor.*, **15**, 1560–1574, <https://doi.org/10.1175/JHM-D-13-0202.1>.
- Qi, S., and F. Luo, 2005: Water environmental degradation of the Heihe River basin in arid Northwestern China. *Environ. Monit. Assess.*, **108**, 205–215, <https://doi.org/10.1007/s10661-005-3912-6>.
- Qin, C., B. Yang, I. Burchardt, X. Hu, and X. Kang, 2010: Intensified pluvial conditions during the twentieth century in the inland Heihe River Basin in arid northwestern China over the past millennium. *Global Planet. Change*, **72**, 192–200, <https://doi.org/10.1016/j.gloplacha.2010.04.005>.
- Seneviratne, S. I., and Coauthors, 2012: Changes in climate extremes and their impacts on the natural physical environment. *Managing the Risks of Extreme Events and Disasters to Advance Climate Change Adaptation*, C. B. Field et al., Eds., Cambridge University Press, 109–230.
- Shangguan, W., and Coauthors, 2013: A China data set of soil properties for land surface modeling. *J. Adv. Model. Earth Syst.*, **5**, 212–224, <https://doi.org/10.1002/jame.20026>.
- Sun, T., J. Wang, Q. Huang, and Y. Li, 2016: Assessment of water rights and irrigation pricing reforms in Heihe River basin in China. *Water*, **8**, 333, <https://doi.org/10.3390/w8080333>.
- Tan, M., and L. Zheng, 2017: Different irrigation water requirements of seed corn and field corn in the Heihe River Basin. *Water*, **9**, 606, <https://doi.org/10.3390/w9080606>.
- Tian, Y., T. Yue, L. Zhu, and N. Clinton, 2005: Modeling population density using land cover data. *Ecol. Modell.*, **189**, 72–88, <https://doi.org/10.1016/j.ecolmodel.2005.03.012>.
- Torrence, C., and G. P. Compo, 1998: A practical guide to wavelet analysis. *Bull. Amer. Meteor. Soc.*, **79**, 61–78, [https://doi.org/10.1175/1520-0477\(1998\)079<0061:APGTWA>2.0.CO;2](https://doi.org/10.1175/1520-0477(1998)079<0061:APGTWA>2.0.CO;2).
- Van Loon, A. F., 2013: On the propagation of drought. How climate and catchment characteristics influence hydrological drought development and recovery. Ph.D. dissertation, Wageningen University, 210 pp., <http://edepot.wur.nl/249786>.
- , 2015: Hydrological drought explained. *Wiley Interdiscip. Rev.: Water*, **2**, 359–392, <https://doi.org/10.1002/wat2.1085>.
- , and H. A. J. Van Lanen, 2012: A process-based typology of hydrological drought. *Hydrol. Earth Syst. Sci.*, **16**, 1915–1946, <https://doi.org/10.5194/hess-16-1915-2012>.
- , E. Tjiedeman, N. Wanders, H. A. J. Van Lanen, A. J. Teuling, and R. Uijlenhoet, 2014: How climate seasonality modifies drought duration and deficit. *J. Geophys. Res. Atmos.*, **119**, 4640–4656, <https://doi.org/10.1002/2013JD020383>.
- , and Coauthors, 2016: Drought in the Anthropocene. *Nat. Geosci.*, **9**, 89–91, <https://doi.org/10.1038/ngeo2646>.
- Wan, W., and Coauthors, 2017: Hydrological drought in the Anthropocene: Impacts of local water extraction and reservoir regulation in the U.S. *J. Geophys. Res. Atmos.*, **122**, 11 313–11 328, <https://doi.org/10.1002/2017JD026899>.
- Wang, G., J. Xia, and J. Chen, 2009: Quantification of effects of climate variations and human activities on runoff by a monthly water balance model: A case study of the Chaobai River basin in northern China. *Water Resour. Res.*, **45**, W00A11, <https://doi.org/10.1029/2007WR006768>.
- Wang, J., H. Li, and X. Hao, 2010: Responses of snowmelt runoff to climatic change in an inland river basin, Northwestern China, over the past 50 years. *Hydrol. Earth Syst. Sci.*, **14**, 1979–1987, <https://doi.org/10.5194/hess-14-1979-2010>.
- Wang, X., and X. Gao, 2002: Sustainable development and management of water resources in the Hei River basin of north-west China. *Int. J. Water Resour. Dev.*, **18**, 335–352, <https://doi.org/10.1080/07900620220135139>.
- Wang, X. F., M. G. Ma, G. H. Huang, F. Veroustraete, Z. H. Zhang, Y. Song, and J. Tan, 2012: Vegetation primary production estimation at maize and alpine meadow over the Heihe River

- Basin, China. *Int. J. Appl. Earth Obs.*, **17**, 94–101, <https://doi.org/10.1016/j.jag.2011.09.009>.
- Wilhite, D. A., 2000: Drought as a natural hazard: Concepts and definitions. *Drought: A Global Assessment*, D. A. Wilhite, Ed., Routledge, 3–18.
- Williams, A. P., R. Seager, J. T. Abatzoglou, B. I. Cook, J. E. Smerdon, and E. R. Cook, 2015: Contribution of anthropogenic warming to California drought during 2012–2014. *Geophys. Res. Lett.*, **42**, 6819–6828, <https://doi.org/10.1002/2015GL064924>.
- Wu, J., Y. Ding, R. Chen, G. Wang, and Y. Shen, 2005: The variation and utilization of water resources in the Heihe River basin. *WIT Trans. Ecol. Environ.*, **80**, 331–339.
- , X. Chen, L. Gao, H. Yao, Y. Chen, and M. Liu, 2016: Response of hydrological drought to meteorological drought under the influence of large reservoir. *Adv. Meteor.*, **2016**, 2197142, <https://doi.org/10.1155/2016/2197142>.
- Xi, H., Q. Feng, J. Si, Z. Chang, and S. Cao, 2010: Impacts of river recharge on groundwater level and hydrochemistry in the lower reaches of Heihe River Watershed, northwestern China. *Hydrogeol. J.*, **18**, 791–801, <https://doi.org/10.1007/s10040-009-0562-8>.
- Xia, J., A. Ye, and G. Wang, 2005a: A distributed time-variant gain model applied to Yellow River (I): Model theories and structures (in Chinese). *Eng. J. Wuhan Univ.*, **38**, 10–15.
- , G. Wang, G. Tan, A. Ye, and G. H. Huang, 2005b: Development of distributed time-variant gain model for nonlinear hydrological systems. *Sci. China Ser. D*, **48**, 713–723, <https://doi.org/10.1360/03yd0183>.
- Ye, A., Q. Duan, H. Zeng, L. Li, and C. Wang, 2010: A distributed time-variant gain hydrological model based on remote sensing. *J. Resour. Ecol.*, **1**, 222–230, <https://doi.org/10.3969/j.issn.1674-764x.2010.03.005>
- , X. Deng, F. Ma, Q. Duan, Z. Zhou, and C. Du, 2017: Integrating weather and climate predictions for seamless hydrologic ensemble forecasting: A case study in the Yalong River basin. *J. Hydrol.*, **547**, 196–207, <https://doi.org/10.1016/j.jhydrol.2017.01.053>.
- Yuan, X., M. Zhang, L. Wang, and T. Zhou, 2017: Understanding and seasonal forecasting of hydrological drought in the Anthropocene. *Hydrol. Earth Syst. Sci.*, **21**, 5477–5492, <https://doi.org/10.5194/hess-21-5477-2017>.
- Zhang, Y. F., 2009: Land use and land cover change in the mid-stream of Heihe River basin and its environmental effect. M.S. thesis, College of Geography and Environmental Science, Xibei Normal University, 63 pp.
- Zhang, Y. Y., 2008: Research and development of joint operation system of cascade reservoirs in the upstream of Heihe River. M.S. thesis, Key Laboratory of Northwest Water Resources and Environmental Ecology, Xi'an University of Technology, 83 pp.
- Zhao, N., T. Yue, W. Shi, X. Zhou, Y. Liu, and Z. Du, 2017: Downscaling simulation of annual average temperature and precipitation of CMIP5 outputs by using HASM – A case study in Heihe River basin. *J. Desert Res.*, **37** (6), 1227–1236.
- Zhao, Y., and J. Zhu, 2015: Assessing quality of grid daily precipitation datasets in China in recent 50 years (in Chinese). *Plateau Meteor.*, **34** (1), 50–58.